Experimental Tests of Entanglement Models of Rubber Elasticity. 3. Biaxial Deformations

Moshe Gottlieb*

Chemical Engineering Department, Ben-Gurion University of the Negev, Beer Sheva 84105, Israel

Richard J. Gaylord

Polymer Group, Department of Materials Science, University of Illinois at Urbana-Champaign, Urbana, Illinois 61801. *Received February 7, 1986*

ABSTRACT: The relative abilities of eight molecular models to describe the response of a cross-linked polymer network to general biaxial deformations are tested. The reduced two-parameter models of Flory and Erman and Ball, Doi, Edwards, and Warner and, to a more limited extent, the reduced one-parameter Gaylord model are found to be able to account for large portions of the published experimental data. However, none of the eight models can reproduce the negative W_2 values that are observed at very small strains. It is shown that the reduced curve method of Treloar for the representation of biaxial data is inferior to the traditional Rivlin–Saunders method.

Introduction

A large number of theoretical models have been proposed during the past few years to describe the response of cross-linked amorphous polymer networks to deformations. These models differ considerably in their treatment of entanglements and network topology and their effect on network behavior. We have undertaken to compare the predictive abilities of as many of these models as possible in describing different types of deformation experiments in order to identify those models that are the most successful and which therefore most correctly account for entanglement effects on elastomeric behavior.

In the first paper of this series[1] uniaxial deformation was examined. It was concluded that (1) a large range of deformation encompassing extension as well as compression is a prerequisite for model testing since almost any reasonable three-parameter model can fit uniaxial extension data and (2) uniaxial deformation behavior is described by several physically different models with about the same degree of success, thereby preventing any conclusion to be reached based on this type of deformation alone.

In the second paper[2] we examined isotropic deformation by swelling. It was found that only a small number of models showed even a qualitative match to the experimentally observed behavior, and none was capable of achieving a quantitative fit to the data.

In the present work biaxial deformations are considered. The molecular models that we tested are the same as the ones we have examined previously[1,2] and include the phantom,[3] affine,[4] and Flory–Erman[5] junction fluctuation models, the Ball–Doi–Edwards–Warner[6] slip-link model, the Edwards[7] primitive path model, and the Gaylord[8] and Marrucci[9] tube models. The Graessley primitive path model,[10] which was considered in our previous papers, is not included here because of its excessively complicated mathematical formulation for a general multiaxial deformation. In addition to these molecular models (a detailed description of which was previously given[2]), we include here the phenomenological Mooney–Rivlin equation[11] because of its widespread use in the literature.

Theory

The deformation behavior of a homogeneous, isotropic, and elastic material is customarily described in terms of the changes in the strain energy density function W and the three principal strains or extension ratios λ_1, λ_2, and λ_3 along a set of orthogonal axes. If the material is assumed to be incompressible, the third strain invariant

$$I_3 = \prod_{i=1}^{3}\lambda_i \tag{1}$$

equals one. The strain energy density function can then be determined by the two remaining invariants of the Cauchy–Green deformation tensor[11,13]

$$W = W(I_1,I_2) \tag{2}$$

where

$$I_1 = \sum_{i=1}^{3}\lambda_i^2 \tag{3}$$

$$I_2 = \sum_{i=1}^{3}\lambda_i^{-2} \tag{4}$$

The true stresses for an incompressible material are obtained from[13,14]

$$t_1 = 2(\lambda_1^2 - \lambda_3^2)(W_1 + \lambda_2^2 W_2) \tag{5}$$

$$t_2 = 2(\lambda_2^2 - \lambda_3^2)(W_1 + \lambda_1^2 W_2) \tag{6}$$

or inversely

$$W_1 = \frac{1}{2}\left(\frac{\lambda_1^2 t_1}{\lambda_1^2 - \lambda_3^2} - \frac{\lambda_2^2 t_2}{\lambda_2^2 - \lambda_3^2}\right)(\lambda_1^2 - \lambda_2^2)^{-1} \tag{7}$$

$$W_2 = -\frac{1}{2}\left(\frac{t_1}{\lambda_1^2 - \lambda_3^2} - \frac{t_2}{\lambda_2^2 - \lambda_3^2}\right)(\lambda_1^2 - \lambda_2^2)^{-1} \tag{8}$$

where $W_k = \partial W/\partial I_k$ for $k = 1$ and 2. In a biaxial deformation experiment, the stresses that are applied to the material are measured as a function of the generated deformations. Using eq 7 and 8, one can determine the derivatives of the strain energy function as functions of I_1 and I_2. It should be pointed out that as a result of incompressibility, only the differences of principal stresses can be determined. Additionally, for the two limiting experimental deformation conditions, uniaxial deformation ($\lambda_2 = \lambda_3 = \lambda_1^{-1/2}$) and equal biaxial deformation ($\lambda_1 = \lambda_2$), eq 7 and 8 are undefined. The appropriate relations for these two cases have been developed by Jones and Treloar[15] and are discussed in more detail in Appendix A.

Valanis and Landel[16] (V–L) have postulated that the strain energy density function is separable into three independent functions of the principal extension ratios

$$W = \sum_{i=1}^{3} w(\lambda_i) \tag{9}$$

Consequently

0024-9297/87/2220-0130$01.50/0

$$t_i - t_j = \lambda_i w'(\lambda_i) - \lambda_j w'(\lambda_j) \tag{10}$$

where $w'(\lambda)$ stands for $\partial w/\partial\lambda$. The V–L hypothesis has been tested by Jones and Treloar[15] and by Vangerko and Treloar[17] and has been found to work well at moderate strains but to be unreliable beyond threefold deformations in either direction. Slightly more restrictive limits have been determined by Kawabata and Kawai.[18]

Finally, the small-strain modulus (or equilibrium modulus) G_0 may be computed from either of the following two relations:

$$G_0 = \lim_{I_1,I_2\to 3} (2W_1 + 2W_2) \tag{11a}$$

$$G_0 = \lim_{\lambda\to 1} \left[\frac{1}{2} \frac{\partial}{\partial\lambda}[\lambda w'(\lambda)] \right] \tag{11b}$$

In our model testing, we want to circumvent the yet unresolved controversy[19–21] regarding the contributions of topological entanglements to the value of the modulus and, instead, concentrate on the strain-dependent predictions of the models. We will therefore reduce all relevant quantities by the modulus value predicted by the model being tested. These moduli values are listed in the second column of Table I.

Treloar Reduced Curve (TRC) Method. The results of biaxial experiments are obtained in the form of the two stress differences at various λ_1 and λ_2 values which are customarily converted by means of eq 7 and 8 into values of the two derivatives of the strain energy density function W_1 and W_2 as functions of I_1 and I_2. Representation of the data in this manner (we shall refer to this method of data representation as the Rivlin–Saunders (RS) method[14]) is cumbersome[14,15,18] and makes model comparison with data difficult.[22] Treloar[23] has recently proposed a method that allows the representation of all biaxial experimental data by one reduced master curve. Within the range of applicability of the V–L hypothesis, curves of $t_1 - t_2$ vs. λ_1 or $t_3 - t_2$ vs. λ_3 at different λ_2 values overlap by means of a vertical shift to form a master curve. This procedure has been successfully tested on a number of different vulcanized rubber samples[15,17] and it has also been shown to hold theoretically[15] for any V–L type expression for W. Since the curves can be shifted vertically to any arbitrary λ_2 value, the value of $\lambda_2 = 1$ corresponding to pure homogeneous shear is selected. For the purpose of model testing, we use the data of Vangerko and Treloar[17] on vulcanized rubber with 5% sulfur, which shows good agreement with previously published data[15] on similar material tested by a different experimental technique over a smaller range of deformations. The data are accurately represented by an Ogden[24] type three-term series:[17]

$$\lambda w'(\lambda) - c = \sum_k \mu_k(\lambda^{\alpha_k} - 1) \tag{12a}$$

$$= [7.525 \times 10^5(\lambda^{1.2947} - 1) + 4.74 \times 10^3(\lambda^{4.7808} - 1) - 4.49 \times 10^3(\lambda^{-2.5505} - 1)] \text{ Pa} \tag{12b}$$

where c is defined as $w'(1)$. From eq 11b we obtain

$$G_0 = \tfrac{1}{2}\sum_k \mu_k\alpha_k \tag{13a}$$

$$= 5.042 \times 10^5 \text{ Pa} \tag{13b}$$

It immediately follows from eq 10 that for $\lambda_2 = 1$

$$t_1 - t_2 = \lambda_1 w'(\lambda_1) - c \tag{14a}$$

$$t_3 - t_2 = -t_2 = \lambda_3 w'(\lambda_3) - c \tag{14b}$$

or

$$f(\lambda) = \lambda w'(\lambda) - w'(1) \tag{15}$$

Table I
Theoretical Expressions for the Tested Models

model[a]	G_0[b]	$\lambda w'(\lambda)/G_0$	W_1/G_0	W_2/G_0	fitted parameters
1. phantom[3]	ξkT	λ^2	$1/2$	0	
2. affine[4]	νkT	λ^2	$1/2$	0	
3. Mooney–Rivlin[11]	$2C_1 + 2C_2$	$A\lambda^2 - (1 - A)\lambda^{-2}$ $A = C_1/(C_1 + C_2)$	$A/2$	$(1 - A)/2$	A
4. Edwards[7]	$\mu kT\Phi/6$ $\Phi = 6 + 2\beta + \alpha^2/(1 - \alpha)$	irreducible to the Valanis–Landel form	$\left[\frac{2(1-\alpha)}{(1-\alpha J)} + \frac{\alpha J(1-\alpha)}{(1-\alpha J)^2} - \frac{\alpha(1-\alpha)}{J(1-\alpha J)} + 4 + 2\beta/J\right]/2\Phi$ $J = (I_1/3)^{1/2}$	0	α, β
5. Ball–Doi–Edwards–Warner[6]	$\mu kT[1 + N_s/(1 + \eta)^2]$	$[A + (1 - A)(1 + \eta)^2 \times (1 + 2\eta + \eta^2\lambda^2)(1 + \eta\lambda^{-2})\lambda^2$ $A = [1 + N_s/(1 + \eta)^2]^{-1}$	eq 7 and 10	eq 8 and 10	A, η (suggested value $\eta = 0.2343343\ldots$)
6. Marrucci[9]	$\nu kT(\alpha + \beta - 1/6(\mu/\nu))$ $\alpha = 2/3(l_0^2/n)$ $\beta = 1/3(rl_0^2/n)$	irreducible to the Valanis–Landel form	$1/2[A + (B/J) + (1 - A - B)/J^2]$ $A = \alpha(\alpha + \beta - 1/6(\mu/\nu))^{-1}$ $B = \beta(\alpha + \beta - 1/6(\mu/\nu))^{-1}$ $J = (I_1/3)^{1/2}$	0	A, B
7. Gaylord[8]	$\nu kT(\alpha + \beta/4)$ $\alpha = sl_0^2/nb^2$ $\beta = 2\pi^2nb^2r/9a_0^2$	$[A + 2(1 - A)\lambda^{-1}]\lambda^2 - B$ $A = \alpha/(\alpha + 1/4\beta)$ $B = 1/6(\alpha + 1/4\beta)$	eq 7 and 10	eq 8 and 10	A
8. Flory–Erman[5]	$\xi kT\Phi$ $\Phi = 1 + \frac{\mu}{\xi}\frac{1 + \kappa^2}{(1 + \kappa)^4}\frac{\kappa^2}{4}(2 - \xi)^2$	$[1 + (\mu/\xi)K(\lambda)]\lambda^2/\Phi$ $K(\lambda) = \frac{B}{1 + B}\frac{\partial B}{\partial(\lambda^2)} + \frac{Bg}{1 + Bg}\frac{\partial(Bg)}{\partial(\lambda^2)}$	eq 7 and 10	eq 8 and 10	κ, ζ $\mu/\xi = 1$

[a] For model details and meanings of parameters, refer to original papers or ref 2. [b] ξ = network cycle rank; ν = number of network strands; μ = number of network junctions.

Table II
Best-Fit Parameter Values

model	reduced biaxial (TRC) parameters	reduced biaxial (TRC) rms[a] × 10^3	biaxial (W_1,W_2), RS method parameters	biaxial (W_1,W_2), RS method rms[a] × 10^3	uniaxial (W_1,W_2) parameters	uniaxial (W_1,W_2) rms[a] × 10^3	pure shear[f] parameters	pure shear[f] rms[a] × 10^3
phantom[3]		91		8.6				41
Mooney–Rivlin[11]	A = 0.96	53	A = 0.83	2.8	A = 0.57	115	A = 0.54	41
Edwards[7]	α = 0.15	52	α = 0.42	4.8			α = 0.62, β = 875	43
	β = 1.84		β = 38					
Ball–Doi–Edwards–Warner[6]	A = 0.88	43	A = 0.75	0.54	A = 0.58, η = 0.18	75	A = 0.62, η = 1.17	15
	η = 2.97		η = 0.59					
	A = 0.86	67[b]	A = 0.66	1.6[b]			A = 0.52	18[b]
Marrucci[9]	A = 2.36	54[c]	A = 1.84	4.5[c]			A = 2.51, B = −4.92	12[c]
	B = −4.66		B = 0.04					
	A = 0.70	78[d]					A = 0.24	25[d]
Gaylord[8]	A = 0.78	66	A = 0.43	1.1	A = 0.32	80	A = 0.13	18
Flory–Erman[5]	κ = 1.6	49	κ = 4.1	0.60	κ = 23, ζ = 0.02	72	κ = 6.8, ζ = 0.2	10
	ζ = 0.38		ζ = 0.004					
	κ = 1.1	52[e]	κ = 4.4	0.61[e]			κ = 7.4	15[e]

[a] The value of rms was calculated by $(1/N)[\sum_{i=1}^{N}(y_{exptl} - y_{calcd})^2]^{1/2}$, where N is the number of experimental points and y_{exptl} and y_{calcd} are the experimental and calculated values, respectively. For second column eq 16 is used. [b] Fit was obtained by fixing η = 0.2343343 as recommended by the authors and adjusting A to get lowest rms value. [c] Best fit to data obtained with physically unacceptable parameters (see text). [d] Fit was obtained by fixing B = 0.5. [e] For comparison purposes fit was obtained by fixing ζ = 0 and fitting the remaining parameter κ to yield lowest rms value. [f] Parameter values were obtained from uniaxial data on same sample.

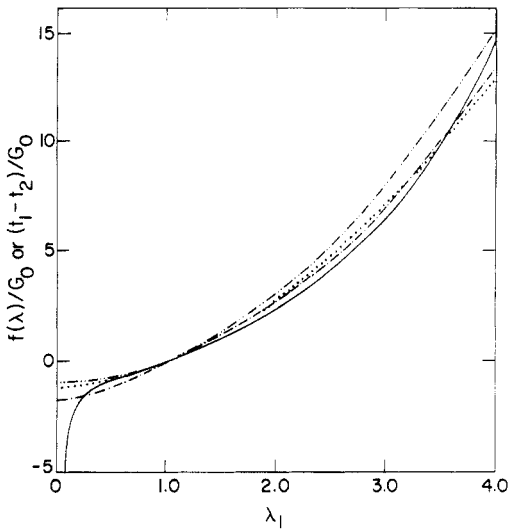

Figure 1. Biaxial extension data plotted according to the TRC method: solid curve, experimental data of Vangerko and Treloar[17] (5% sulfur); dotted line, Gaylord model;[8] dash–dot line, Flory–Erman model;[5] dash–double-dot line, phantom[3] and affine[4] models.

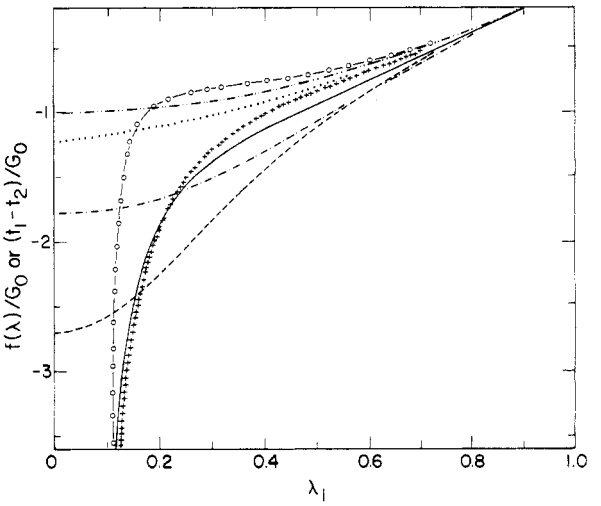

Figure 2. Details of the TRC method curves at small extension values: dashed line, BDEW model;[6] dash–circle line, Edwards model;[7] crossed line, Mooney–Rivlin equation.[11] All other curves are the same as in Figure 1.

The experimental differences $(t_1 - t_2)/G_0$ or $(t_3 - t_2)/G_0$ can be plotted in terms of eq 12 (reduced by eq 13) as a function of λ_1 (or λ_3).

Six of the eight molecular models can be expressed in the form of a V–L type strain energy density function. The appropriate $\lambda w'(\lambda)/G_0$ expressions are given in the third column of Table I. These can be directly plotted vs. λ and compared to the experimental curve. The Edwards[7] primitive path model (also the Graessley[10] primitive path model) and the Marrucci[9] tube model cannot be reduced to a V–L form. Therefore, in order to obtain values of $(t_1 - t_2)/G_0$ at $\lambda_2 = 1$ for these two models, as required in the TRC method, the strain energy function derivatives with respect to I_1 and I_2 for these models are computed (see columns 4 and 5 of Table I) and then eq 5 and 6 are used with $\lambda_2 = 1$ and $\lambda_3 = 1/\lambda_1$.

The best-fit parameters for the different models are obtained by applying the Levenberg–Marquardt[25] method to one hundred "experimental" points computed from eq 12 in the interval $0.1 \leq \lambda \leq 4.0$. Since by definition, $f(\lambda) = 0$ for $\lambda = 1$, only 20 points were chosen in the interval $^2/_3 \leq \lambda \leq {}^3/_2$. The remaining points were placed equidistantly along the rest of the interval. A relative magnitude best-fit criterion was employed requiring the minimization of an objective function of the form

$$M = \min \{ \sum_{\substack{\text{all} \\ \text{points}}} [(y_{exptl} - y_{calcd})/y_{exptl}]^2 \} \qquad (16)$$

The parameter values and the average root mean square (rms) value ($=M^{1/2}/$(number of points)) for the various models are shown in columns two and three of Table II. The calculated theoretical curves are compared to experiment in Figures 1 and 2. The manipulated and smoothed experimental data of Vangerko and Treloar[17] are depicted by the solid line in both figures. In Figure 1 the entire range of extension values is shown. In Figure 2 the lower range of extension ($\lambda < 1.0$) is redrawn in greater detail. For clarity sake, only four theoretical curves are shown in Figure 1: the affine[4] and phantom[3] junction fluctuation models, whose curves are identical, the Flory–Erman[5]

Table III
Limiting Values of the TRC Function as $\lambda \to 0$

model	$\lim_{\lambda \to 0} [f(\lambda)/G_0]$	model	$\lim_{\lambda \to 0} [f(\lambda)/G_0]$
phantom	−1	BDEW	$[(A-1)(\eta^2+2\eta)]-1$
affine	−1	Marrucci	$-A$
Mooney–Rivlin	$-\infty$	Gaylord	$A-2$
Edwards	$-\infty$ at $J = 1/\alpha$	Flory–Erman	$-(1+\mu/\xi)/\Phi$, $\kappa > 0$ -1, $\kappa = 0$

model, and the Gaylord[8] model. The first and last of these three curves form upper and lower bounds respectively in the high-deformation range. The rest of the models (not shown) will all lie between these two curves in this interval. The agreement between the theoretical and experimental curves is quite satisfactory, with the largest deviation in the vicinity of $\lambda = 2.5$, amounting to 26% for the affine and phantom models and 11% for the Flory–Erman model. The combined experimental and numerical errors (due to the superposition scheme) have been estimated[15,17] at 6–9%, larger than the differences between predictions of most models for $\lambda > 1.0$.

The situation is quite different at the lower end of the strain range, depicted in Figure 2, where a very sharp downturn of the experimental data is observed at $\lambda < 0.3$. Six of the eight models fail to show this behavior because they approach finite limiting values of $f(\lambda)$ as $\lambda \to 0$ (these values are given in Table III). On the other hand, in the Ogden series representation of the data (eq 12b), the last term dominates the series at small λ values, with $f(\lambda)$ approaching $-\infty$ as $\lambda \to 0$. As Table III indicates, only the Mooney–Rivlin equation[11] and the Edwards[7] model with an appropriate α value show this trend.

A possible molecular origin of this downturn is finite chain extensibility, as has been argued by Treloar.[23] In the Edwards model,[7] this arises naturally from the depletion of the surplus segment population. Riding and Treloar[26] have incorporated the finite extensibility effect into the phantom model and have argued that a non-V–L form is necessary in order to display the downturn. In both the Edwards and Riding–Treloar models, the fit with experiment at higher strains (low λ values) is achieved at the expense of the fit at lower strains. Kovac and Crabb[27] have incorporated the finite extensibility effect into the Gaylord model, which is then more successful than the other two models in fitting the entire range of λ values. It is important to recognize that in addition to the effect of finite chain extensibility, strain-induced crystallization has also been identified[28] as a possible cause for the observed low-λ behavior. The uncertainty[23,29,30] regarding the origin and importance of the observed downturn of the data at low λ values and the apparent success of the otherwise inadequate Mooney–Rivlin equation in displaying this behavior indicate that the adequacy of a model cannot be determined solely on the basis of its ability to predict this downturn. Hence, the goodness of fit over the entire strain range as measured by the average rms will be used to compare the merits of the models tested here.

Inspection of the second column in Table II reveals that the BDEW model with the η parameter value tenfold larger than suggested by its authors[6] has the lowest rms value (0.043). This value increases considerably (0.067) when the suggested $\eta = 0.23433$ value is used, in which case the curve is virtually indistinguishable from the phantom curve in Figure 2 and only slightly above the Flory–Erman curve in Figure 1. A slightly higher rms value (0.049) is obtained with the Flory–Erman model with a ζ value somewhat larger than suggested by its authors.[31,32] Setting ζ equal to zero results in minor changes in the rms and κ values. The Edwards model (0.052), the Mooney–Rivlin equation (0.053), and the Marrucci model (0.054) all have almost identical rms values. For the Marrucci model, this rms value results from using a physically unrealistic negative β parameter obtained by the regression analysis. When a positive β (or B) value is imposed, the quality of fit deteriorates considerably. A somewhat higher rms value (0.066) is obtained by the Gaylord model. The worst fit is achieved by the phantom and affine models.

While the TRC method provides a simple computational scheme by which to test molecular models in describing the otherwise unwieldy biaxial stress data, there is a question as to the accuracy of the TRC method in the representation of multiaxial stress behavior.

The rather extensive body of experimental data on biaxial deformations[14,15,18,23,33,34] shows unambiguously that the strain energy density function W is a function of I_2 (i.e., $W_2 \neq 0$) and the derivatives of W with respect to I_1 or I_2 are not constant but, rather, functions of both strain invariants. The TRC method is incapable of distinguishing between models that do or do not show these behaviors; this fact is clearly demonstrated by the results presented above. Of the five models having the lowest rms values, the Edwards and Marrucci models predict $W_2 = 0$ (cf. Table I) and the Mooney–Rivlin equation predicts constant W_1 and W_2 values (yet the Edwards model and Mooney–Rivlin equation are unique in reproducing the observed downturn at small λ values). Additionally, the Mooney–Rivlin equation, which has long been known to be unable to correctly describe even the relatively simple uniaxial deformation experiment[5,18,21] in compression and at above-moderate extension, appears to be successful by the TRC method because the entire uniaxial extension–compression curve is represented by the point $\lambda = 1.0$, for which, by definition, all models yield $f(\lambda) = 0$.

From these facts, we have to conclude that although the TRC method is very attractive in its simplicity, it is not a useful tool as for the evaluation of rubber elasticity models. We therefore turn to another scheme.

Rivlin–Saunders (RS) Method. Since the TRC method is not adequate, we resort to the more cumbersome RS method of representing the data in the form of W_1 and W_2 as functions of I_1 and I_2. Graphically, four sets of plots are required, one for each strain energy derivative–strain invariant pair. Each plot is composed of a series of curves at fixed values of the remaining strain invariant. The data of Jones and Treloar[15] are depicted in this manner in Figures 3 and 4 by solid lines which represent the reduced strain energy derivatives as a function of I_j ($j = 1, 2$) for fixed I_k ($k \neq j$). The contour lines for a fixed I_k value are usually a decreasing function of I_j except for the case of W_1 as a function of I_1 for high I_2 values (>10). In the latter case, W_1 increases with I_1, and this trend becomes progressively more pronounced as I_2 increases.[17,23] The origin of the upward swing of the curves is probably the same as that causing the downward swing in the curves of the TRC method at low λ values. The trends shown in Figures 3 and 4 also occur in the earlier work of Rivlin and Saunders,[14] including the upward swing at high I_1 and I_2 (although it is less pronounced due to large experimental scatter). The relative magnitudes of W_1 and W_2 are similar in both works, despite the variance in absolute values due to differences in network structure. The general trends observed by Jones and Treloar are supported by Obata et al.[33] and Kawabata et al.[34] but the details differ, especially at the low-deformation end of the experimental range (I_1, $I_2 < 3.5$). This point will be discussed in more detail in the next section.

Table IV
Comparison between Theoretical and Experimental Values at Low and High Extension Values

		W_1/G_0						W_2/G_0				
I_1	I_2	exptl[15]	F–E[5]	Gaylord[8]	BDEW[6]	Edwards[7]	Kawabata[34]	exptl[15]	F–E[5]	Gaylord[8]	BDEW[6]	Kawabata[34]
3.000	3.000	0.416	0.405	0.429	0.410	0.500	0.685	0.0839	0.0954	0.0712	0.0902	−0.185
3.400	3.318	0.410	0.404	0.421	0.405	0.474	0.476	0.0788	0.0852	0.0667	0.0819	0.046
	3.400	0.409	0.403	0.421	0.404	0.474	0.430	0.0783	0.0839	0.0662	0.0811	0.089
	3.517	0.408	0.402	0.420	0.403	0.474	0.384	0.0776	0.0821	0.0656	0.0798	0.121
11.0	28.0	0.372	0.361	0.338	0.370	0.385		0.0264	0.0161	0.0199	0.0142	
	29.85	0.371	0.360	0.337	0.370	0.385		0.0257	0.0155	0.0193	0.0134	
	30.45	0.370	0.360	0.336	0.370	0.385		0.0255	0.0153	0.0191	0.0132	
3.318	3.400	0.410	0.403	0.422	0.404	0.479	0.395	0.0789	0.0846	0.0667	0.0819	0.116
3.400		0.409	0.403	0.421	0.404	0.474	0.430	0.0839	0.0839	0.0662	0.0811	0.089
3.517		0.408	0.404	0.419	0.404	0.467	0.481	0.0828	0.0828	0.0656	0.0799	0.035
8.89	20.00	0.368	0.369	0.349	0.371	0.353		0.0322	0.0208	0.0250	0.0195	
9.25		0.370	0.368	0.348	0.371	0.354		0.0318	0.0206	0.0247	0.0193	
9.77		0.372	0.367	0.346	0.372	0.359		0.0313	0.0204	0.0243	0.0191	

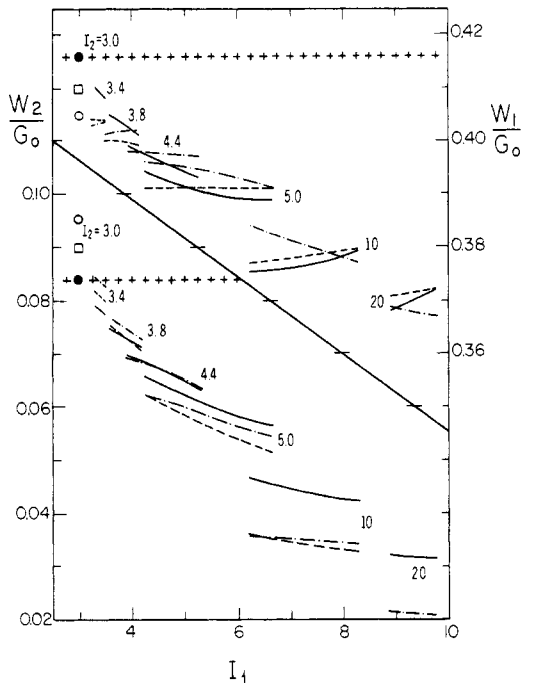

Figure 3. Reduced $\partial W/\partial I_1$ and $\partial W/\partial I_2$ vs. I_1: solid lines and filled circles, experimental data of Jones and Treloar;[15] dash–dot lines and open circles, Flory–Erman model;[5] crossed lines, Mooney–Rivlin equation;[11] dashed lines and squares, BDEW model.[6]

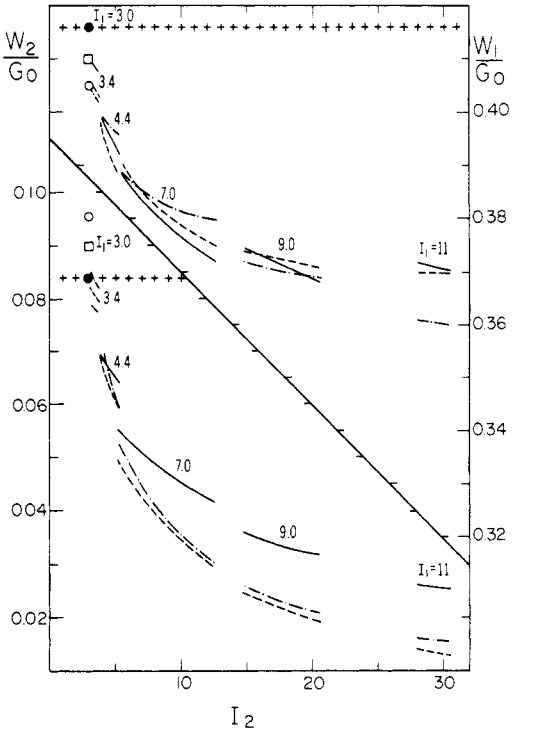

Figure 4. Reduced $\partial W/\partial I_1$ and $\partial W/\partial I_2$ vs. I_2. Curves are the same as in Figure 3.

The experimental curves in Figures 3 and 4 are composed of 108 points, which were used simultaneously to obtain the absolute least-squares parameter estimates by the procedure described in the previous section. The results of the regression analyses are shown in the fourth and fifth columns of Table II. A comparison of the third and fifth columns in Table II shows that deficiencies inherent in the TRC method (relatively small differences between the rms values of the different models and the illusory success of the Edwards and Marrucci models and the Mooney–Rivlin equation) are not present in the RS method.

The best fit to the data, as determined by the rms value, is obtained by the BDEW and the Flory–Erman models. Setting $\zeta = 0$ in the latter has only a minor effect on the quality of fit. The values of the fitted parameters are similar to those obtained for natural rubber[22] and PEA.[31] In the BDEW case, the use of the suggested $\eta = 0.23433$ value results in a considerable reduction in the quality of fit. A rms value 2 times larger than those for the Flory–Erman and BDEW models is obtained in fitting the Gaylord model. The best fit for the Marrucci model requires a physically unrealistic parameter value ($\beta \approx 0$), and when a positive β is imposed on the model, the rms value increases by an order of magnitude and is almost identical with the one obtained by the phantom network model, which has no adjustable parameters.

The predictions of the BDEW model, the Flory–Erman model, and the Mooney–Rivlin equation are depicted in Figures 3 and 4. The trends of the experimental contour lines are always reproduced by the BDEW model and with one exception (W_1 vs. I_1) by the Flory–Erman model. Good quantitative agreement is observed for intermediate strains but relatively large discrepancies are observed at higher strains ($I_2 > 10$) and at relatively small deformations ($I_i < 3.5$). This latter disagreement is undetectable by the TRC method due to the basic definition of $f(\lambda)$ at $\lambda = 1$.

The predictions of four models in the low- and high-deformation ranges are compared to experimental values in Table IV. From this table, it is evident that the BDEW model is the most successful in matching the data of Jones and Treloar[15] at small strains. The BDEW model is also in better agreement with experimental values of W_1 at high strains but deviates considerably when W_2 values are considered. In the latter the Gaylord model is in better

agreement with experiment.

As already pointed out, the Flory–Erman model predicts correctly the trends of the experimental contour lines with only one exception—the curves of W_1/G_0 as a function of I_1 (Figure 3). At small strains, the Flory–Erman model predicts that W_1 increases with I_1, contrary to experiment. The trends shown in Table IV for the other three models agree with the Jones and Treloar data but the data of Kawabata et al.[34] (also in Table IV) support the Flory–Erman prediction. This point will be discussed in the next section. In the intermediate strain range in Figure 3 the agreement between theory and experiment is reestablished only to be reversed at higher strains. Here, the Flory–Erman model predicts that W_1 decreases as I_1 increases whereas experiments show the opposite trend. This discrepancy becomes larger as I_1 and I_2 increase, as shown in Figure 3 as well as in ref 23, where a wider strain range is considered[17] (up to $I_2 = 150$). Table IV shows that the correct trend is predicted by the Edwards and BDEW models but not by the Gaylord model. As I_1 and I_2 increase beyond $I_1 = 15$ and $I_2 = 40$, the trend of increasing W_1 with I_1 becomes more pronounced,[23] in agreement with the Edwards model but in contrast to the prediction of the BDEW model. The source of this behavior is the same as that of the downturn seen with the TRC method. The ability of the Edwards model to mimic that downturn (shown in Figure 2) is duplicated here by its prediction of the correct trends at high strains. However, this ability is considerably outweighed by the inability of the Edwards model to obtain nonzero W_2 values.

Values of $\lambda_1 \approx 0.22$ in Figure 2 correspond to $I_2 = 20$ in Table IV. At this point, the TRC curve of the BDEW model agrees with the experimental TRC curve and hence with the experimental trends shown in Table IV but as I_2 is increased (smaller λ_1 value in Figure 2), the BDEW predictions depart from experiment.

Small-Strain Behavior. Kawabata, Kawai, Obata, and co-workers[18,33,34] have studied the behavior of rubbers under multiaxial deformation, paying special attention to very careful measurements at small strains, a region characterized by a great sensitivity to experimental errors. Their results agree with those obtained by others[14,15,17] at intermediate and high strains ($I_1 > 4.5I_2 > 7$) but differ considerably in several respects at lower strains. The contour lines in Figures 3 and 4 show that on the basis of the data of Jones and Treloar[15] (supported by Rivlin and Saunders[14] and Vangerko and Treloar[17]), W_1 and W_2 are decreasing functions of both I_1 and I_2 at low deformations. The data of Kawabata and co-workers show the same trend for W_1 vs. I_2 and W_2 vs. I_1 but the opposite trend for W_1 vs. I_1 and W_2 vs. I_2. These trends are partially reproduced by the Flory–Erman model, as can be seen in Table IV, although the quantitative fit is poor. Furthermore, a very sharp increase in W_1 and decrease in W_2 is observed at $I_j < 3.1$, yielding negative values of W_2 in the vicinity of $I_j = 3.0$. This peculiar behavior is observed under uniaxial,[18] equibiaxial,[34] and intermediate biaxial deformation conditions. Neither Rivlin and Saunders[14] nor Treloar and co-workers[15,17] observed this sort of behavior. However, their positive W_2 values at $I_j = 3.0$ were obtained by extrapolating from the W_2 values measured at deformations that were much higher than the point of inclination observed by Kawabata et al.,[18,34] and it is therefore not surprising that they did not see any deviation from the trend they observed at the higher strains. None of the models mimic this experimental behavior, as indicated by the values in the first row of Table IV.

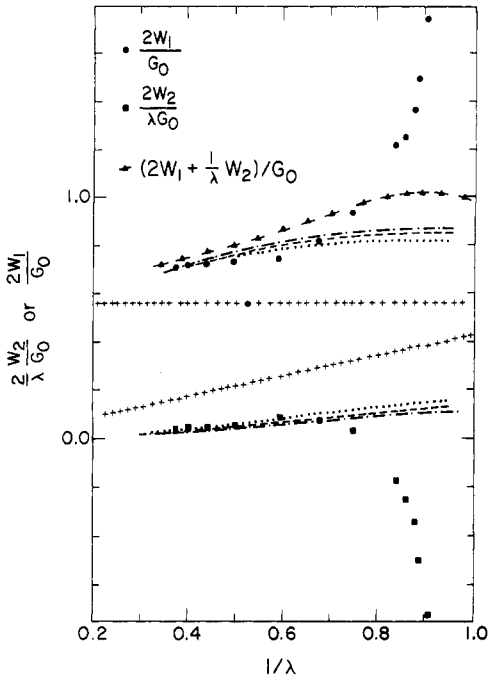

Figure 5. Mooney plot of simple elongational data and the contribution of the two strain invariant derivatives. Experimental data are from Kawabata and Kawai;[18] theoretical curves are the same as in Figure 2.

In order to further investigate this problem, we examine the uniaxial extension data of Kawabata and Kawai.[18] These data, in the customary form of the Mooney plot of $t_1/(\lambda_1^2 - \lambda_1^{-1})G_0$ vs. $1/\lambda$, are depicted by triangles in Figure 5. Parameters for the different models were obtained by best fitting the data. The resulting parameter values obtained by using 12 experimental points are given in Table II under the "uniaxial (W_1, W_2)" heading (models yielding $W_2 = 0$ are not considered here). From eq 5, it follows that

$$\frac{t_1}{\lambda_1^2 - \lambda_1^{-1}} = 2W_1 + \frac{1}{\lambda}2W_2 \tag{17}$$

We now proceed to compute W_1/G_0 and W_2/G_0 separately by means of eq A3 and A4, using these parameter values. These computed values are compared to the reduced W_1 and W_2 experimental values that were independently measured by Kawabata and Kawai and which are indicated, after proper reduction, by the circles and squares, respectively, in Figure 5. The average deviation of the computed $2W_1$ and $2W_2/\lambda$ values from the experimental points are represented by the rms values in the seventh column of Table II. The best agreement (lowest rms) is obtained by the Flory–Erman model. The sharp increase in $2W_1$ values and the negative $2W_2/\lambda$ values at small strains are not reproduced by any of the models. Furthermore, it can be shown (see Appendix C) that W_2 is always positive for physically realistic positive parameter values in the case of uniaxial deformation for the BDEW and Gaylord models (no such proof has been attempted for the Flory–Erman model due to its algebraic complexity). Behavior similar to that shown for uniaxial deformation in Figure 5 has also been reported by Kawabata et al.[34] in pure shear experiments. Here again, $2W_1$ and $2W_2$ show a sharp upturn and downturn, respectively, as $I_1 = I_2 \rightarrow 3.0$ but the sum of the two is almost unchanged. It is unlikely that any of the models will be able to reproduce this behavior either. Negative W_2 values and behavior similar to that described above have also been reported for small-strain biaxial deformations[35] and torsion

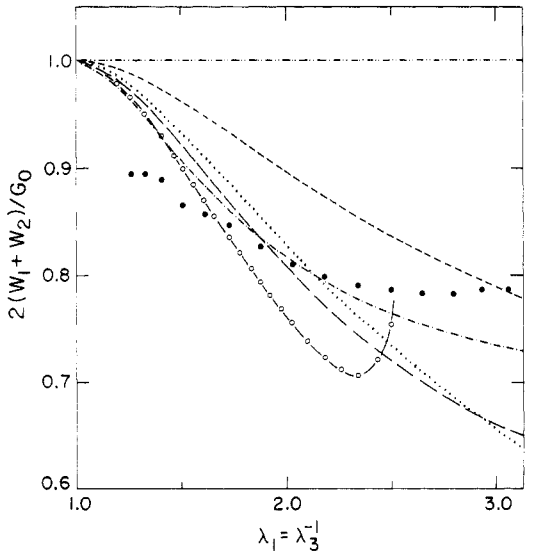

Figure 6. Comparison between experimental pure shear data and model predictions, employing parameters obtained from uniaxial extension data on the same material. Solid circles, experimental data of Rivlin and Saunders;[14] short-dash line, BDEW model[6] with η = 1.373; long-dash line, BDEW model with η = 0.2343343; the rest of curves are the same as in Figure 2.

experiments[36,37] in some cases but not in others.[38]

Finally, Figure 5 demonstrates the flaws in the Mooney–Rivlin equation (as has also been pointed out by many other researchers[14,15,18]). It is obvious that its apparent success in describing uniaxial extension data over intermediate extensions stems from the fortuitous parallelness of the W_1 and W_2/λ lines over that region which does not hold at either higher or lower deformations. Furthermore, W_1 is clearly not constant and therefore cannot be identified with C_1 in the Mooney–Rivlin equation while the W_2 contribution is considerably smaller than that attributed to it by the Mooney–Rivlin C_2 parameter. Therefore, any attempt to assign a molecular interpretation to the empirical parameters of the equation are foredoomed. Finally, the extrapolation of Mooney–Rivlin type plots to the $1/\lambda \rightarrow 0$ limit is quite dubious.

Combined Uniaxial and Pure Shear Experiments. The most meaningful test of a molecular model is its ability to correctly describe deformation behavior under a given type of deformation using material parameters obtained from another type of deformation. Since these parameters usually depend on the sample structure, it is essential that both experiments be performed on identical samples. Unfortunately, only a few such experimental studies have been reported. Rivlin and Saunders[14] performed uniaxial and pure shear experiments on specimens obtained from the same sheet of vulcanized rubber (their sample A). We have used their uniaxial deformation data to obtain the parameters for the various models and then to compare the theoretical predictions to the experimental data for pure shear. The results are reported in Figure 6 with the parameter values and quality of fit to the shear data given in the last two columns of Table II. None of the models follow the data over the entire experimental range. The large degree of uncertainty in the small-deformation data of both uniaxial and pure shear experiments may be partially responsible for this relatively poor agreement. The best fit is obtained by the Flory–Erman model followed by the BDEW and Gaylord models. The best-fit parameter values are similar to the ones obtained for the general biaxial data.

Conclusion

In this paper, we have examined the relative abilities of eight molecular models to describe polymer network response to a variety of deformations. The theoretical equations were expressed in a reduced form in order to bypass the small-strain-modulus controversy. No model was capable of reproducing all of the experimental observations over the entire experimental range. The two-parameter models of Flory and Erman and BDEW were best able to account for most of the experimental results while the one-parameter model of Gaylord achieved a somewhat more limited success. The other models were much less successful than these three models.

In the three tests by which the models were evaluated, the predictions of the Flory–Erman and BDEW models were generally in 50–100% better agreement with data, as measured by the rms value, than those of the Gaylord model. The parameters of the Flory–Erman model obtained by the regression analyses were in good agreement with published values.[5,22,31,32,39,42] The value of the ζ parameter was close to zero and, except for the pure shear experiment, had little effect on the quality of fit. In the BDEW model, the η parameter varied considerably for the different data sets and was usually much larger than the 0.23433 value suggested by its authors while the A parameter had values within the range 0.6–0.75 for all of the experiments and for all values of η. The sole parameter in the Gaylord model varied to a large extent for the different tests. While the Marrucci model showed good agreement with the data when no constraints were imposed on the value of its parameters, this best fit was always achieved by using physically unacceptable negative or zero parameter values, and imposing positive parameter values on the fitting resulted in a very poor correlation to the data, which was often as poor as that of the phantom and affine models. The Edwards model also showed a relatively poor data fitting capability even when using, in some instances, physically unrealistic parameter values. It was noted that the Marrucci and Edwards models also predict a zero W_2 value, in conflict with all available experimental findings, and they also cannot be expressed in terms of the V–L formulation. It seems, therefore, that these two models are much less desirable choices for modeling polymer network deformation behavior.

We have shown that although mathematically and graphically attractive, the Treloar reduced curve method for representing biaxial data is quite inferior to the Rivlin–Saunders method and may lead one to incorrect conclusions regarding the relative merits of various models.

Finally, the well-known inapplicability of the phenomenological Mooney–Rivlin equation to the interpretation of the strain energy function determination and the lack of physical meaning associated with its empirical parameters has once again been demonstrated.

Two major issues that merit further attention can be pointed out here: the peculiar behavior of the two strain energy derivatives at very low deformations[40] and at high strain. Both issues require further experimental investigation. Most importantly, experimental data on identical, well-characterized specimens exposed to several different types of deformation are essential for the testing of the comparative predictive abilities of molecular models.

Finally, while we have concentrated here on the best-fit abilities of the molecular models, there are other criteria that are equally important in choosing between models, including conceptual acceptability and the mathematical simplicity of the theoretical development and the final expression (including the number of adjustable parame-

Table V
Expressions for $f'(\lambda)/G_0$ Necessary To Obtain W_1 and W_2 at Experimental Limits[a]

model	$f'(\lambda)/G_0$
BDEW	$2A\lambda + 2(1-A)(1+\eta)^2\lambda(1+2\eta-\eta\lambda^2)(1+\eta\lambda^2)^{-3}$
Gaylord	$2A\lambda + 2(1-A)$
Flory-Erman[b]	$\frac{2\lambda}{\Phi} + \frac{2\mu}{\xi}\frac{\lambda}{\Phi}K(\lambda) + \frac{\mu}{\xi}\frac{\lambda^2}{\Phi}\frac{\partial K(\lambda)}{\partial\lambda}$

[a] Refer to Table 1 for nomenclature. [b] For the evaluation of this equation, refer to Appendix B.

ters). These points will be addressed later on in this series of papers.

Acknowledgment. Support for this work was provided in part by the NSF, Polymers Program. Professor Burak Erman was helpful in pointing out a simplified notation for Appendix B.

Appendix A. Computation of W_1 and W_2 for Uniaxial and Equibiaxial Deformations

The equations used to compute the two strain energy density derivatives, eq 7 and 8, are indeterminate for the two limiting deformations $\lambda_2 = \lambda_3 = \lambda_1^{-1/2}$ (uniaxial) and $\lambda_1 = \lambda_2$ (equal biaxial). Since eq 7 and 8 are used in conjunction with eq 10 for the computation of W_1 and W_2 in the case of the BDEW, Gaylord, and Flory–Erman models, approximate relations are used for these limiting cases. The details of the derivation are given by Jones and Treloar[15] and we limit ourselves to providing the relationships necessary for the evaluation of these terms for these three models.

1. Simple Uniaxial Extension

$$t_2 = t_3 = 0 \qquad \lambda_2 = \lambda_3 = \lambda_1^{-1/2} \tag{A1}$$

From eq 10 with application of eq A1 we find

$$t_1 = \lambda_1 w'(\lambda_1) - \lambda_1^{-1/2} w'(\lambda_1^{-1/2}) \tag{A2}$$

Following Jones and Treloar,[15] we obtain

$$\lim_{\lambda_2\to\lambda_3} W_2 = -\frac{1}{2}\left[\frac{t_1}{\lambda_1^2 - \lambda_1^{-1}} - \frac{f'(\lambda^{-1/2})}{2\lambda_1^{-1/2}}\right](\lambda_1^2 - \lambda_1^{-1})^{-1} \tag{A3}$$

$$\lim_{\lambda_2\to\lambda_3} W_1 = \frac{1}{2}\left(\frac{t_1}{\lambda_1^2 - \lambda_1^{-1}} - \frac{2W_2}{\lambda_1}\right) \tag{A4}$$

where $f'(\lambda) = \partial[\lambda w'(\lambda)]/\partial\lambda$. Expressions for $f'(\lambda)/G_0$ for the three models are given in Table V.

2. Equal Biaxial Extension

$$t_3 = 0 \qquad t_1 = t_2 \qquad \lambda_1 = \lambda_2 = \lambda_3^{-1/2} \tag{A5}$$

From eq 10 and A5

$$t_1 = t_2 = \lambda_1 w'(\lambda_1) - \lambda_1^{-2} w'(\lambda_1^{-2}) \tag{A6}$$

and

$$\lim_{\lambda_1\to\lambda_2} W_2 = -\frac{1}{2}\left(\frac{f'(\lambda_1)}{2\lambda_1} - \frac{t_1}{\lambda_1^2 - \lambda_1^{-2}}\right)(\lambda_1^2 - \lambda_1^{-2})^{-1} \tag{A7}$$

$$\lim_{\lambda_1\to\lambda_2} W_1 = \frac{1}{2}\left(\frac{t_1}{\lambda_1^2 - \lambda_1^{-2}} - 2\lambda_1^2 W_2\right) \tag{A8}$$

Here again $f'(\lambda_1)$ is obtained from Table V. Equations A2 and A6 are evaluated with the aid of the expressions given in the third column of Table I and thus W_1 and W_2 can be computed for both limiting cases.

Appendix B. Evaluation of the Flory–Erman Expression

As a result of the algebraic complexity of this model, we give here the complete expressions necessary for the evaluation of eq A3 and A7.

Define the operator $\dot{x} = \partial x/\partial\lambda^2$; then

$$K(\lambda) = \frac{B\dot{B}}{B+1} + \frac{B^2\dot{g}g + g^2B\dot{B}}{1+Bg} \tag{B1}$$

where[5]

$$B = (\lambda - 1)[1 + \lambda - \zeta\lambda^2](1+g)^{-2} \tag{B2}$$

$$g = \lambda^2[\kappa^{-1} + \zeta(\lambda - 1)] \tag{B3}$$

$$\dot{g} = \kappa^{-1} - \zeta(1 - 3\lambda/2) \tag{B4}$$

$$\dot{B} = B\left[\frac{1}{2\lambda(\lambda-1)} + \frac{1-2\lambda\zeta}{2\lambda(1+\lambda-\zeta\lambda^2)} - \frac{2\dot{g}}{1+g}\right] \tag{B5}$$

From these definitions it follows that

$$\ddot{g} = \frac{\partial\dot{g}}{\partial\lambda^2} = \frac{3}{4}\frac{\zeta}{\lambda} \tag{B6}$$

$$\ddot{B} = \frac{\partial\dot{B}}{\partial\lambda^2} = (2\lambda)^{-1}\left\{\dot{B}\left[\frac{1}{\lambda-1} + \frac{1-2\lambda\zeta}{1+\lambda-\zeta\lambda^2} - \frac{4\lambda\dot{g}}{1+g}\right] - B\left[\frac{2\lambda-1}{2\lambda^2(\lambda-1)^2} + \frac{1+\lambda-\zeta\lambda^2+\lambda(1-2\lambda\zeta)^2}{2\lambda^2(1+\lambda-\zeta\lambda^2)^2} + \frac{3\zeta(1+g) - 4\lambda\dot{g}^2}{(1+g)^2}\right]\right\} \tag{B7}$$

$$\dot{K} = \frac{\dot{B}^2 + B^2\ddot{B} + B\ddot{B}}{(1+B)^2} + \frac{(B\dot{g} + \dot{B}g)^2}{(1+Bg)^2} + \frac{Bg(B\ddot{g} + 2\dot{B}\dot{g} + \ddot{B}g)}{(1+Bg)} \tag{B8}$$

Finally

$$\frac{f'(\lambda)}{G_0} = \frac{2\lambda}{\Phi}\left[1 + \left(\frac{\mu}{\xi}\right)K(\lambda)\right] + \frac{2\lambda^3}{\Phi}\left(\frac{\mu}{\xi}\right)\dot{K} \tag{B9}$$

where Φ is defined in Table I.

Appendix C. Proof of the Positive Value of W_2 for the Gaylord and BDEW Models

It is obvious that the Mooney–Rivlin equation is incapable of showing the respective upturn and downturn behavior in W_1 and W_2/λ at low strains (see Figure 5). We can also show that neither the BDEW nor the Gaylord model predicts negative W_2 values at small strain in uniaxial deformation.

1. Gaylord Model. By inserting the appropriate terms from Table I (row 7, column 2) into eq A2 and from Table V into eq A3, we obtain

$$\frac{W_2}{G_0} = -\frac{1}{2}(1-A)\frac{(2\lambda^{1/2} - \lambda^{-1} - \lambda^2)}{(\lambda^2 - \lambda^{-1})^2}\lambda^{1/2} = \frac{1}{2}(1-A)\frac{(\lambda - \lambda^{-1/2})^2}{(\lambda^2 - \lambda^{-1})^2}\lambda^{1/2} \tag{C1}$$

Thus, for $A \leq 1$, $W_2/G_0 \geq 0$ for any λ. Additionally

$$\lim_{\lambda\to 1}(W_2/G_0) = (1-A)/8 \tag{C2}$$

2. BDEW Model. The positive value of W_2/G_0 in uniaxial deformation can be shown by the procedure used

above, but first, a somewhat simpler method will be employed. Kearsley and Zapas[37] have shown that for uniaxial deformation, the limiting value of W_2 in terms of the V–L function is

$$\lim_{\lambda\to 1} W_2 = \frac{1}{16}\left\{\frac{\partial w(\lambda)}{\partial\lambda} - \frac{\partial^2 w(\lambda)}{\partial\lambda^2} - \frac{\partial^3 w(\lambda)}{\partial\lambda^3}\right\}_{\lambda=1} \quad \text{(C3)}$$

From the second column in Table I we find

$$\frac{1}{G_0}\frac{\partial w}{\partial\lambda} = A\lambda + (1-A)(1+\eta)^2(1+2\eta+\eta^2\lambda^2)\lambda(1+\eta\lambda^2)^{-2} \quad \text{(C4)}$$

Inserting the derivatives of eq C4 into eq C3, we obtain

$$\lim_{\lambda\to 1}\frac{W_2}{G_0} = (1-A)\left\{(1+\eta)\eta - 2\eta^2 + \frac{\eta^3}{1+\eta}\right\} = (1-A)\eta/(1+\eta) \quad \text{(C5)}$$

Thus for $A \leq 1$ and $\eta \geq 0$ the limiting value of W_2/G_0 is positive.

Using the procedure employed for the Gaylord model calculation, it is possible to show, after tedious algebraic manipulation, that

$$\frac{W_2}{G_0} = -\frac{1}{2}\frac{(1-A)(1+\eta)^2\eta}{(1+\eta\lambda^{-1})^3(1+\eta\lambda^2)^2(\lambda^2-\lambda^{-1})^2}\{2(-\lambda^4+2\lambda-\lambda^{-2}) + \eta(-\lambda^6-3\lambda^4+2\lambda^3+6\lambda-1-3\lambda^{-2}) + \eta^2(-2\lambda^6+\lambda^5+3\lambda^3-2\lambda^2+\lambda^{-1}-\lambda^{-3})\} \quad \text{(C6)}$$

and thus $W_2/G_0 > 0$ when $\eta > \lambda/(1-2\lambda)$. Hence, in the case of uniaxial extension ($\lambda > 1$), W_2/G_0 is positive at all strains for any $A < 1$ and $\eta > 0$. The value of W_2 can become negative at high compressions ($\lambda < {}^1/_2$) for certain choices of η.

References and Notes

(1) Gottlieb, M.; Gaylord, R. J. *Polymer* **1983**, *24*, 1644.
(2) Gottlieb, M.; Gaylord, R. J. *Macromolecules* **1984**, *17*, 2024.
(3) James, H. M. *J. Chem. Phys.* **1947**, *15*, 651. James, H. M.; Guth, E. *Ibid.* **1947**, *15*, 669.
(4) Flory, P. J. *J. Chem. Phys.* **1950**, *18*, 108.
(5) Flory, P. J.; Erman, B. *Macromolecules* **1982**, *15*, 800.
(6) Ball, R. C.; Doi, M.; Edwards, S. F.; Warner, M. *Polymer* **1981**, *22*, 1010.
(7) Edwards, S. F. *Br. Polym. J.* **1977**, *9*, 140.
(8) Gaylord, R. J. *Polym. Bull. (Berlin)* **1982**, *8*, 325; **1983**, *9*, 181.
(9) Marrucci, G. *Macromolecules* **1981**, *14*, 434.
(10) Graessley, W. W. *Adv. Polym. Sci.* **1982**, *46*, 67.
(11) Mooney, M. *J. Appl. Phys.* **1940**, *11*, 582. Rivlin, R. S. *Philos. Trans. R. Soc. London, A:* **1948**, *A241*, 379.
(12) Tschoegl, N. W.; Gürer, C. *Macromolecules* **1985**, *18*, 680.
(13) Rivlin, R. S. *Philos. Trans. R. Soc. London, A:* **1949**, *A242*, 173.
(14) Rivlin, R. S.; Saunders, D. W. *Philos. Trans. R. Soc. London, A:* **1951**, *A243*, 251.
(15) Jones, D. F.; Treloar, L. R. G. *J. Phys. D: Appl. Phys.* **1975**, *8*, 1285.
(16) Valanis, K. C.; Landel, R. F. *J. Appl. Phys.* **1967**, *38*, 2997.
(17) Vangerko, H.; Treloar, L. R. G. *J. Phys. D: Appl. Phys.* **1978**, *11*, 1969.
(18) Kawabata, S.; Kawai, S. *Adv. Polym. Sci.* **1977**, *24*, 90.
(19) Queslel, J. P.; Mark, J. D. *Adv. Polym. Sci.* **1984**, *65*, 135.
(20) Gottlieb, M.; Macosko, C. W.; Benjamin, G. S.; Meyers, K. O.; Merrill, E. W. *Macromolecules* **1981**, *14*, 1039.
(21) Eichinger, B. E. *Annu. Rev. Phys. Chem.* **1983**, *34*, 359.
(22) Erman, B. *J. Polym. Sci., Polym. Phys. Ed.* **1981**, *19*, 829.
(23) Treloar, L. R. G. *Br. Polym. J.* **1982**, *14*, 121.
(24) Ogden, R. W. *Proc. R. Soc. London, Ser. A* **1972**, *A326*, 565.
(25) Brown, K. M.; Dennis, J. E. *Numer. Math.* **1972**, *18*, 289. Also IMSL Reference Manual, IMSL Inc., Houston, TX, 1979; p ZXSSQ-1.
(26) Riding, G.; Treloar, L. R. G. *Proc. R. Soc. London, Ser A:* **1979**, *A369*, 261.
(27) Kovac, J.; Crabb, C. C. *Macromolecules* **1986**, *19*, 1744.
(28) Mark, J. E. *Polym. Eng. Sci.* **1979**, *19*, 254; *Adv. Polym. Sci.* **1982**, *44*, 1.
(29) Kosc, M.; Ziabicki, A. *Macromolecules* **1982**, *15*, 1507.
(30) Gee, G. *Macromolecules* **1980**, *13*, 705.
(31) Erman, B.; Flory, P. J. *Macromolecules* **1982**, *15*, 806.
(32) Erman, B. *J. Polym. Sci., Polym. Phys. Ed.* **1983**, *21*, 893.
(33) Obata, Y.; Kawabata, S.; Kawai, H. *J. Polym. Sci., Part A-2* **1970**, *8*, 903.
(34) Kawabata, S.; Matsuda, M.; Tei, K.; Kawai, H. *Macromolecules* **1981**, *14*, 154.
(35) Zapas, L. J. *J. Res. Natl. Bur. Stand., Sect. A* **1966**, *70A*, 525.
(36) Penn. R. W.; Kearsley, E. A. *Trans. Soc. Rheol.* **1976**, *20*, 227.
(37) Kearsley, E. A.; Zapas, L. J. *J. Rheol.* **1980**, *24*, 483.
(38) McKenna, G. B.; Zapas, L. J. *Polymer* **1983**, *24*, 1495.
(39) McKenna, G. B.; Hinkley, J. A. *Polymer*, submitted.
(40) Peculiar small-strain behavior reported recently[41] and strong dependence on time,[35] aging,[38] and preparation[38] of samples serve to underline the importance of further work on small-strain phenomena.
(41) McKenna, G. B.; Zapas, L. J. *Polymer* **1983**, *24*, 1502.
(42) Brotzman, R. W.; Mark, J. E. *Macromolecules* **1986**, *19*, 667.

Translational Diffusion of Poly(methyl methacrylate) in Acetone: Wormlike vs. Freely Jointed Chain Model

Y. F. Maa and S. H. Chen*

Department of Chemical Engineering, University of Rochester, Rochester, New York 14627.
Received August 6, 1986

ABSTRACT: The translational diffusion coefficients of poly(methyl methacrylate) standards with molecular weights 7.67×10^3, 2.7×10^4, 4.9×10^4, and 6.39×10^4 in acetone at infinite dilution were determined with the extended Taylor dispersion technique at temperatures from 274.2 to 313.2 K. Both wormlike and freely jointed chain models were found to represent quite well the experimental results, suggesting that the excluded volume effects on the hydrodynamic radii are virtually absent. The scaling relationship between diffusivity and molecular weight was verified, and a proportionality of D to $TM^{-0.49}/\mu_0$ was also established.

Introduction

Translational diffusioin coefficients of chainlike polymers in extremely dilute solution carry significant information on the hydrodynamic behavior of isolated macromolecules. Although a variety of macromolecular models have been advanced over the years, understanding of conformational characteristics at the molecular level relies on relevant experimental observation to which analytical models[1,2] are compared. From the practical point of view, such diffusion data are needed for the analysis of the diffusion-controlled casting of "asymmetric" membrane[3]

*Author to whom correspondence should be addressed.

0024-9297/87/2220-0138$01.50/0